# Symposium-in-Print: Green Fluorescent Protein and Homologs

# (Sub)-Picosecond Spectral Evolution of Fluorescence in Photoactive Proteins Studied with a Synchroscan Streak Camera System

I. H. M. van Stokkum*[1], B. Gobets[1], T. Gensch[2], F. van Mourik[1], K. J. Hellingwerf[1,2], R. van Grondelle[1] and J. T. M. Kennis[1]

[1]Department of Physics and Astronomy, Faculty of Sciences, Vrije Universiteit, Amsterdam, The Netherlands
[2]Department of Microbiology, University of Amsterdam, Amsterdam, The Netherlands

## ABSTRACT

The spectral evolution of three photoactive proteins has been investigated by measuring the fluorescence with good temporal and wavelength resolution and a high signal-to-noise ratio. Upon excitation at 400 nm wild-type (wt) PYP both at neutral pH and in the low-pH blueshifted pBdark state exhibited a strong quenching of the fluorescence, the major part of which could be described by lifetimes of about 1.7 and 7.7 ps. The remaining fluorescence decay occurred multiexponentially with lifetimes between 30 and 125 ps. Additionally, in wtPYP at neutral pH, a dynamic Stokes shift was found to occur with a time constant of about 0.25 ps. In a PYP preparation that was reconstituted with the chromophore 7-hydroxy-coumarin-3-carboxylic acid rather than the native coumaric acid, and which is therefore not capable of performing the cis-*trans*-isomerization that initiates the photocycle in wtPYP, the fluorescence was found to decay multiexponentially with lifetimes of 51 ps, 0.33 and 3.77 ns. Additionally, dynamic Stokes shifts were observed with time constants of about 0.1 and 3.5 ps. Upon comparison of the dynamics of this preparation with that of wtPYP the multiexponential decay with lifetimes of 1.7 and 7.7 ps found in wtPYP was attributed to photochemistry of the p-coumaric-acid chromophore. The emission from bacteriorhodopsin mutant D85S upon excitation at 635 nm decays biexponentially with estimated lifetimes of 5.2 and 19.1 ps. No dynamic Stokes shift was observed here. Four lifetimes were needed to describe the decay of the emission from the A* state in the green fluorescent protein. From a target analysis it was concluded that the longer lifetimes are accompanied by a decreasing probability of forming I*, which approaches zero with the longest A* lifetime of 1.5 ns. These observations may be explained by heterogeneity of A and by relaxation of A*. In all three systems studied, multiexponential decay of emission was present, suggesting that heterogeneity is a common feature of these chromophore protein complexes.

*Corresponding author email: ivo@nat.vu.nl (I. H. M. van Stokkum)

## INTRODUCTION

In nature, organisms use the light in their environment by means of photoactive proteins, which can serve to harvest the energy of incident light, or to sense or transmit information carried by light. Photoactive proteins bind chromophores, which, upon absorption of light, undergo the photochemical or photophysical processes that ultimately lead to the protein's biological function. The sequence of events is often rather complicated: The photochemical processes can occur in a multiexponential way and may branch out to result in different, coexisting reaction products. Moreover, photochemical reactions in photoactive proteins are often so rapid that they compete with vibrational relaxation and solvation processes.

Time-resolved fluorescence spectroscopy is a powerful tool to investigate the dynamical processes that occur in the excited state. Especially when conducted in a spectrally resolved way, detailed information can be obtained on movement on the potential energy surface along reaction or solvation coordinates (1,2), and on the reaction rates to photoproducts.

Little is known of the solvation dynamics in photoactive proteins. Extensive studies have shown that in liquids, two components could be distinguished: a fast inertial response, occurring on a timescale less than 100 fs, followed by a slower, diffusive component on a picosecond timescale (1–4). The inertial response often accounts for half the total reorganization energy or more, and entails independent, underdamped motion of the solvent molecules in their native potential wells. The diffusive component represents the reorientation of the solvent molecules into a new equilibrium, whereby the nuclei may hop between different potential wells. It involves collective motions of solvent molecules, like librations and large rotations. It is thought that the diffusive solvent rearrangement plays an important role in chemical reactivity, as it may reduce reaction barriers and stabilize reaction intermediates. Photon echo and time-resolved fluorescence spectroscopy measurements have indicated that the solvation dynamics in various chromophore-binding proteins is dominated by an inertial response, and no or very small diffusive components could be detected (5–11).

The spectral evolution of three photoactive proteins is investigated in this report with the use of a synchroscan streak camera system in combination with a spectrograph, to monitor the spectral evolution of the emission over a wide spectral range with an

instrument response function (IRF) of 3 ps (FWHM), and a wavelength resolution of 8–12 nm. This system enables us to measure the fluorescence with good temporal and wavelength resolution and a high signal to noise ratio. We chose three model systems: photoactive yellow protein (PYP), the bacteriorhodopsin (bR) mutant D85S, which has a much longer lifetime with respect to that of wtbR, and the (wt) green fluorescent protein (GFP). To obtain additional insights into the dynamics of excited chromophores in PYP, a modified PYP has been constructed where the p-coumaric-acid chromophore was replaced by 7-hydroxy-coumarin-3-carboxylic acid. In this system, *trans*-cis isomerization is precluded, and we further refer to it as *locked PYP*. GFP displays photochemistry with two emissive states, and thus the modeling of this photochemistry called for the use of target analysis. On the contrary, PYP and D85S show photochemistry with only one single emissive state. Therefore in these cases the photochemistry, or nonradiative decay to a ground-state intermediate, could be inferred directly from the decay of the emission. The time resolution, after iterative reconvolution with the IRF, is sufficient to monitor processes on timescales of 0.3 ps to 3 ns. The acquired data consist of matrices containing a total of 30–50 000 points, which are analyzed globally, thus providing precise parameter estimation. We aim to quantify the multiexponentiality of emission decay in these chromophore–protein complexes, the possible solvation induced shifts of the emission spectrum, and the photochemistry of GFP.

## MATERIALS AND METHODS

*Experimental setup.* The streak camera system and measurement procedures were described in detail in (12). Here we will only address the main features and the parameters and settings specific for these measurements. For the excitation of the samples we either used 400 nm light obtained by frequency-doubling the (800 nm) light from the Mira-RegA (Coherent, Santa Clara, CA) oscillator/regenerative amplifier combination, 635 nm light obtained from the optical parametric amplifier (Coherent OPA) which was pumped by the Mira-RegA system, or 377 nm light obtained by mixing the 713 nm output of the OPA with part of the 800 nm from the Mira-RegA combination. The pulses possessed a spectral width of about 10 nm FWHM, a length of about 200 fs, and a spot size of 100–150 μm. The pulses were attenuated with a variable neutral density filter. The fluorescence was collected at right angle to the exciting light, and focused into a spectrograph (Chromex IS250, Albuquerque, NM). The output of the spectrograph was directed into a synchroscan streak camera (Hamamatsu C5680 and M5675, Hamamatsu City, Japan), and streak images (fluorescence intensity measured both as a function of time and wavelength) were recorded on a Dual Scan Cooled CCD camera (Hamamatsu C4880). The IRF of the entire system measured 2.6–3.5 ps FWHM. Data were accumulated up to 1200 s per streak image (integration on the CCD chip), and up to 8 of such images were averaged. The full wavelength range of a streak image was 315 nm, covering the full emission spectra. The wavelength resolution for the detection was 8 nm, except for the D85S mutant, where it was 12 nm. The full-time range was 200 ps for the highest time resolution, and 0.8 or 2.2 ns to capture long-lived emission components.

Because of the limited wavelength resolution of the monochromator, the curvature-corrected and averaged images were reduced to a matrix of 1000 points in time and 33 or 44 points in wavelength. The PYP samples were prepared according to the standard procedure described elsewhere (13,14), and were diluted with Tris buffer pH 7.5 (PYP at neutral pH and locked PYP), or buffer pH 2, for PYP at low pH, directly preceding the experiments, to provide an optical density of about 0.5/cm at the absorption maximum. For PYP at neutral pH and locked PYP excitation was at 400 nm, whereas it was at 377 nm for PYP at low pH. The repetition rate was 20 kHz with 20–60 nJ pulses. Excitation light was horizontally polarized, and fluorescence was detected under an angle of 90 degrees, with vertical polarization so as to minimize the detection of scattered light. The sample was contained in a spinning cell with a 3-mm optical path length, rotating at approximately 600 rpm, and was kept at room temperature. Under these conditions each volume was exposed to approximately one excitation pulse during a single passage through the focus.

Absorption spectra were measured before and after each experiment and revealed no noticeable changes. The site-directed mutagenesis technique used to construct the D85S mutant of bR is described elsewhere (15). Membranes of the D85S mutant were dissolved in a 50 m*M* potassium phosphate buffer at pH 6.0. For the time-resolved fluorescence measurements, the suspension was diluted to an optical absorbance of 0.5/cm at 600 nm. Excitation was at 635 nm with 25 nJ pulses at a 20 kHz repetition rate. Excitation was vertical and no polarizer was used for the detection because of the low signal intensity. The sample was pumped through a home-built flow cell (1 × 1 mm square cross section) at a flow rate of 20 mL/min, and was cooled to 287 K. Under these conditions each volume was exposed to fewer than 10 excitation pulses during a single passage through the focus.

Outside of the excitation volume the sample was continuously illuminated with blue light to prevent the possible buildup of a long-lived blue-absorbing state, which has been reported for the spectroscopically similar deionized or acid blue membrane.

For the time-resolved fluorescence measurements, GFP was diluted to an optical absorbance of 0.5/cm with the use of a 10 m*M* Tris buffer at pH 8.0. Excitation was at 400 nm with 50 nJ pulses at a 20 kHz repetition rate. Excitation was either horizontal or vertical (adjusted with a Berek compensator), and detection was vertical, such that anisotropic data were acquired. The wavelength resolution for the detection was 8 nm. The sample was pumped through a home-built flow cell (1 × 1 mm square cross section) at a flow rate of 25 mL/min, and was kept at room temperature. Under these conditions each volume was exposed to fewer than 10 excitation pulses during a single passage through the focus.

*Data analysis.* To describe the spectral evolution a sequential (also termed *unbranched unidirectional*) model (14,16,17) with increasing lifetimes was used to estimate evolution-associated spectra (EAS). When using a target kinetic model the species-associated spectra (SAS) are estimated. The decay-associated spectra (DAS) can be calculated from EAS or SAS by a linear transformation (17). The IRF was described in the global analysis by a Gaussian shape (6). The Raman scattering of water (centered around 467 nm for 400 nm excitation) complicated the PYP measurement. We modeled it as an extra component contributing between 445 and 490 nm, with a time course identical to that of the IRF. When an ultrafast decay was present as well, we could only estimate its amplitude reliably at wavelengths below those of the Raman scattering. We arbitrarily set the contribution of such a component to zero at the other wavelengths. Backsweep signals due to long-lived emission were modeled as in (6).

To further quantify the spectral evolution the SAS, or sometimes also the EAS, are fitted with a spectral model from which the average wave number is calculated. As model function a skewed Gaussian in the energy domain is used (17):

$$\varepsilon(\bar{v}) = \bar{v}^5 f_{max} \exp\left(-\ln(2)\{\ln(1 + 2b(\bar{v} - \bar{v}_{max})/\Delta\bar{v})/b\}^2\right) \qquad (1)$$

where $\bar{v}_{max}$ is the Franck–Condon wave number of maximum emission. The FWHM is given by $\Delta\bar{v}_{1/2} = \Delta\bar{v} \sinh(b)/b$. Note that with skewness parameter $b$ equal to zero the expression simplifies to a Gaussian. The average wave number of this function is given by

$$\bar{v}_{av} = \bar{v}_{max} + \frac{\Delta\bar{v}}{2b}\left(\exp\left(-\frac{3b^2}{4\ln(2)}\right) - 1\right) \qquad (2)$$

Alternatively, solvation could be described with the use of a time-dependent shift of $\bar{v}_{max}$ (2,18). This requires data with a higher time and wavelength resolution, e.g. from fluorescence upconversion (2,4,9) where also higher excitation intensities are necessary. The spectral evolution description used here approximates a gradual change with an average spectral change associated with a time constant.

## RESULTS AND DISCUSSION

### Photoactive yellow protein

*PYP at neutral pH.* The photoactive yellow protein (PYP) (13,20,21) is a small water-soluble protein from the purple sulphur bacterium *Ectothiorhodospira halophila*, containing a thiol-ester linked p-coumaric-acid (pCA) chromophore. The protein exhibits broad absorption and emission bands with maxima at, respectively,

446 and 494 nm, at neutral pH (22). Upon light absorption, the pCA chromophore undergoes a rapid *trans*-cis isomerization, which leads to a deprotonation of the chromophore on a microsecond timescale and, ultimately, to the signaling state in which the protein partially unfolds (23,24). The photochemistry in wtPYP is characterized by subpicosecond to picosecond timescales (19,25–30). Because the PYP chromophore is present in a water-soluble protein, and is shielded from bulk water essentially only by arginine-52, it is of great interest to look for protein-related solvation effects on picosecond timescales as well.

wtPYP at neutral pH was excited at 400 nm, to the blue relative of the absorbance maximum at 446 nm. Global analysis revealed four time constants of about 0.25, 1.7, 7.7, and 49 ps. Typical traces, shown in Fig. 1A,B, reveal that the decay below 450 nm is dominated by a lifetime of about 0.25 ps. The shapes of the EAS in Fig. 1C of these three components resemble each other. Their $\bar{v}_{av}$ were, respectively, 20.1, 20.2 and $20.3 \times 10^3$ cm$^{-1}$, a difference that is hardly significant in view of the imprecision of the spectral parameters. The EAS of the ultrafast (0.25 ps) decaying component (solid line) could not be estimated above 445 nm, and was arbitrarily set to zero.

Earlier fluorescence upconversion studies (27,28) with an IRF of about 200 fs FWHM revealed multiexponential decay in wtPYP with time constants ranging from 0.4 to 10 ps. Time constants ranging from 0.5 to 10 ps were reported in (27), with the use of a 10 ps scan length. In (28) the shortest lifetimes were 0.4–1.0 ps and 3.1–4.3 ps, with the use of a 30 ps time window. We were not able to resolve the two fastest lifetimes in wtPYP. Instead, we found an average of 1.7 ps, and an additional 7.7 ps component. The analysis of these multiexponential decays is further complicated by the presence of slow-decaying components with a low amplitude. We also performed a global analysis of the single photon counting data from (28). This resulted in lifetimes of 2.5 and 27 ps, 0.10, 0.55 and 3.1 ns. The complex multiexponential decay was corroborated by pump-probe studies (17,26,30,31). With the use of a target analysis it was shown that isomerization takes place mainly during the 0.6 and 2.8 ps processes, and hardly on the 40 ps process (30). The excited states that do not enter the photocycle decay to a ground-state intermediate. In accordance with these earlier results, we assign the 1.7 and 7.7 ps components predominantly to a *trans*-cis isomerization process of the pCA chromophore, whereas the 49 ps component represents a fraction that does not undergo isomerization and returns to the ground state via an intermediate on the ground-state potential energy surface (30).

In previous studies (19,27,28) emission was monitored at wavelengths between 445 and 600 nm. Here we have also measured the more blue wavelengths down to 420 nm. Upconversion measurements, upon excitation at 400 nm (19), 423 or 455 nm (27), and 420 nm (28), did not reveal a dynamic Stokes shift in wtPYP. The shortest detection wavelengths reported were 445 nm (19), 468 nm (27), and 455 nm (28). We excited at 400 nm and could observe from 420 nm onwards, which enabled us to reveal the dynamic Stokes shift between 420 and 445 nm, occurring in about 0.25 ps (kinetic trace at 441 nm in Fig. 1A [solid] and the solid EAS in Fig. 1C). This dynamic Stokes shift may be due to the combined effects of vibrational relaxation after excitation in the high-energy side of the PYP absorption band, and inertial solvation phenomena.

*PYP at low pH.* At low pH the coumaric-acid chromophore becomes protonated, resulting in a large blueshift of the absorption and emission spectra (22). For comparison with PYP at neutral pH we also measured the emission of this so called pBdark state of
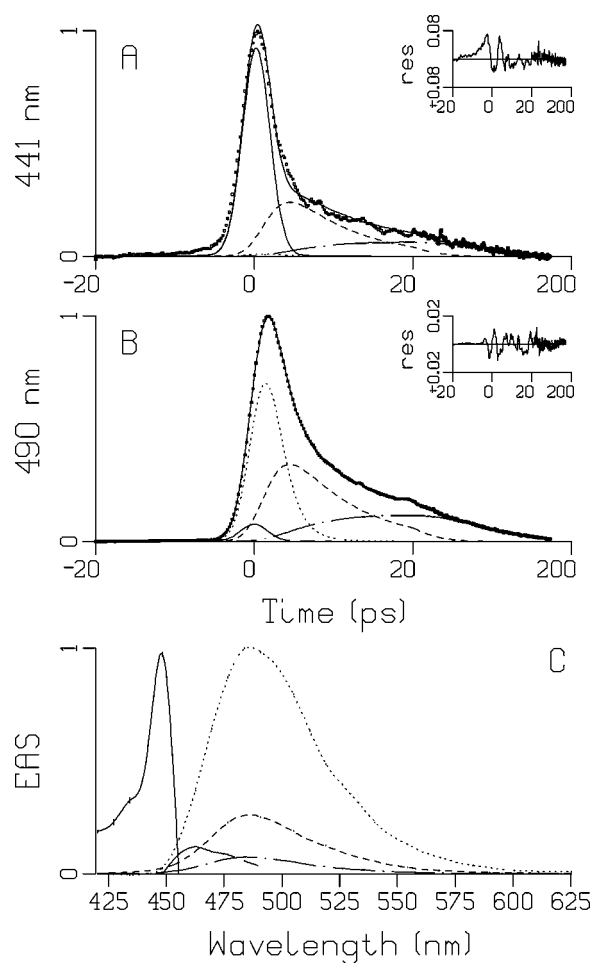


Figure 1. Results from global analysis of wtPYP excited at 400 nm. (A,B) Fit of (normalized) kinetics measured at 441 and 490 nm (indicated at the ordinate). Insets show residuals of a fit with a sequential model with four increasing lifetimes. The contributions of these components to the fit are depicted by different line types. Key: 0.25 ps (solid, fixed), 1.7 ps (dotted), 7.7 ps (dashed), 49 ps (dot-dashed). The sum of these contributions is also represented by a solid line through the measuring points. The time base is linear from −20 to +20 ps (relative to the maximum of the IRF), and logarithmic from 20 to 200 ps. (C) Evolution-associated spectra (EAS). The small chain-dashed curve in (B) straddling time zero represents the contribution of the Raman scatter, which extends from 445 to 490 nm in (C).

PYP. wtPYP in the pBdark state was excited at 377 nm, which, in contrast to the neutral pH measurement, is on the low-energy side relative to the absorbance maximum at 360 nm (at pH 2). Therefore, no vibrational relaxation is expected. However, a Stokes shift due to solvation is still expected to occur. The results are shown in Fig. 2, where the kinetic traces at 407 and 437 nm are depicted (panel A and B, respectively), along with the result of the global analysis (panel C). The wavelength of maximum emission, 432 nm, agrees fairly well with the 439 nm reported in (22), taking into account our 8 nm wavelength resolution. Four lifetimes, 2.1, 10, 34 and 149 ps are required for an adequate description of the time-resolved emission data. In contrast to PYP at neutral pH, no ultrafast component in the order of 0.2 ps was observed here. The two short lifetimes of 2.1 and 10 ps are similar to those found at neutral pH. The slow decay was described by 34 and 149 ps lifetimes. The relative contribution of the 2.1 ps component was largest at short wavelengths (solid lines in Fig. 2A,B). The EAS of
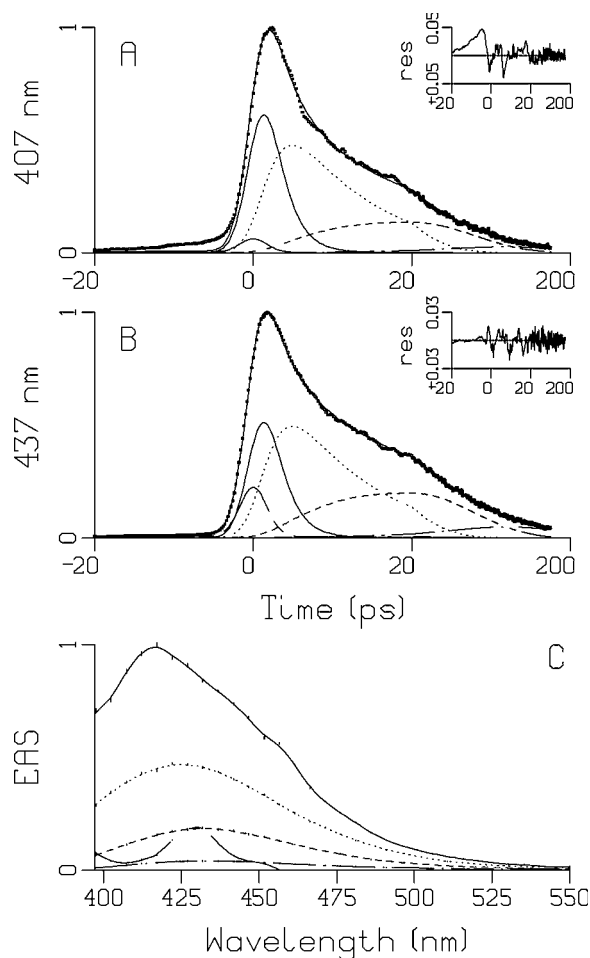
**Figure 2.** Results from global analysis of wtPYP in the pBdark state excited at 377 nm. (A,B) Fit of (normalized) kinetics measured at 407 and 437 nm (indicated at the ordinate). Insets show residuals of a fit with a sequential model with four increasing lifetimes. The contributions of these components to the fit are depicted by different line types. Key: 2.1 ps (solid), 10 ps (dotted), 34 ps (dashed), 149 ps (dot-dashed). The sum of these contributions is also represented by a solid line through the measuring points. The time base is linear from −20 to +20 ps (relative to the maximum of the IRF), and logarithmic from 20 to 200 ps. (C) Evolution-associated spectra (EAS). The small chain-dashed curve in (B) (very tiny in [A]) straddling time zero represents the contribution of the (Raman) scatter, which extends up to 452 nm in (C).

the 2.1 ps component (Fig. 2C, solid line) is somewhat blueshifted relative to the EAS of the three slower decaying components. The $\bar{\nu}_{av}$ were, respectively, 23.0, 22.8, 22.4 and $21.8 \times 10^3$ cm$^{-1}$. In pB$_{dark}$ the small redshift of about 200 cm$^{-1}$ in 2.1 ps is accompanied by a decrease of the EAS (compare solid and dotted curves in Fig. 2C). Comparing to Fig. 1C, the relative decrease with 2.1 ps was smaller. This is interpreted as the absence of photochemistry but presence of a decay pathway to a ground-state intermediate.

*Locked PYP*. Earlier measurements of the decay of the emission in locked PYP revealed that the fastest process in this system exhibits a time constant of about 60 ps (28). The observation that the fast (<15 ps) components that were found in wtPYP are absent in locked PYP confirmed the assignment of these lifetimes in wtPYP to photochemical processes. In the absence of competing photochemical processes, locked PYP thus appears particularly suited to study solvation effects.
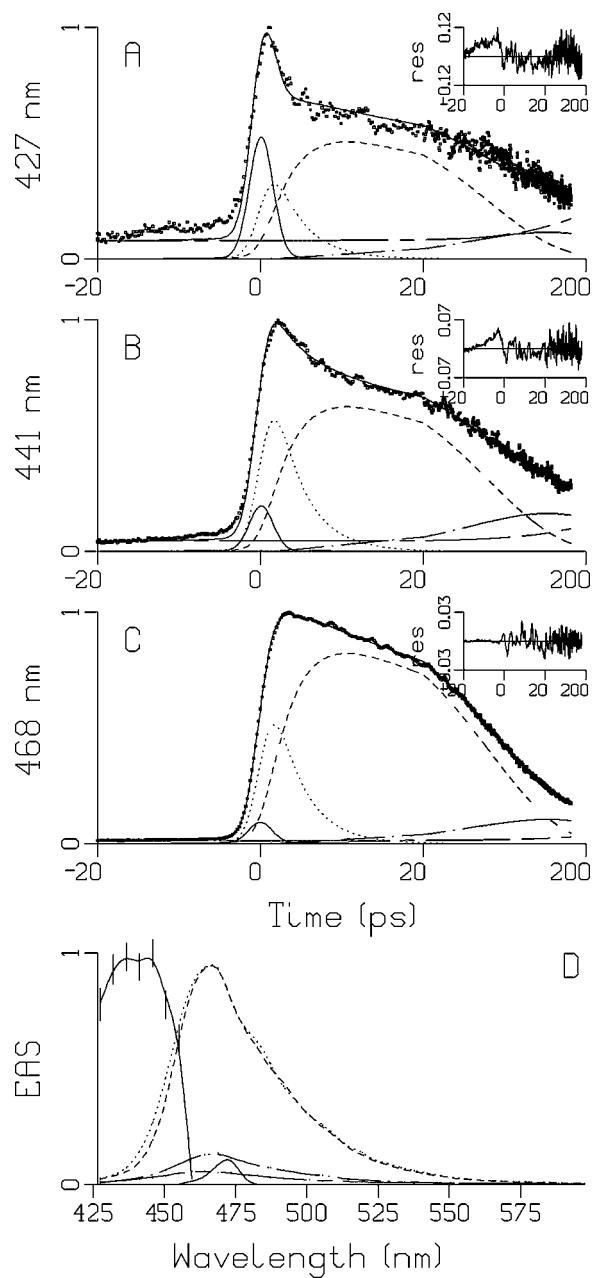
**Figure 3.** Results from global analysis of locked PYP excited at 400 nm. (A,B,C) Fit of (normalized) kinetics measured at 427, 441, and 468 nm (indicated at the ordinate). Insets show residuals of a fit with a sequential model with five increasing lifetimes. The contributions of these components to the fit are depicted by different line types. Key: 0.1 ps (solid, fixed), 3.5 ps (dotted), 51 ps (dashed), 0.33 ns (dot-dashed), 3.77 ns (chain-dashed). The sum of these contributions is also represented by a solid line through the data points. The time base is linear from −20 to +20 ps (relative to the maximum of the IRF), and logarithmic from 20 to 200 ps. (D) Evolution-associated spectra (EAS). The small solid curve in (C) straddling time zero represents the contribution of the Raman scatter, which extends from 456 to 480 nm in (D).

Locked PYP, which absorbs maximally at 443 nm (28), was excited at 400 nm. Representative kinetic traces recorded at 427, 441 and 468 nm are plotted in Fig. 3A–C, and the EAS that result from a sequential analysis of the data are shown in Fig. 3D. The five components that were required to fit the data have lifetimes of 0.1, 3.5, 51, 330 ps, and 3.77 ns.

Figure 3D reveals a major, ultrafast redshift of the fluorescence occurring on a timescale of about 0.1 ps, comparable to the redshift found in wtPYP at neutral pH. Again, the EAS of the ultrafast decaying component (solid line) could not be estimated above 450 nm, and was arbitrarily set to zero. As in PYP at neutral pH, the origin of the dynamic Stokes shift may be the combined effects of vibrational relaxation after excitation in the blue edge of the locked PYP absorption band, and inertial solvation phenomena.

Interestingly, the EAS of the 3.5 ps component is slightly blue-shifted compared to the EAS of the 51 ps component (dotted versus dashed lines in Fig. 3D, in particular from 430 to 450 nm; see also the 441 nm trace in Fig. 3B). The $\bar{\nu}_{av}$ were both $20.8 \times 10^3$ cm$^{-1}$.

Because the areas under the 3.5 and 51 ps EAS are virtually identical (compare dotted and dashed curves in Fig. 3D) we conclude that the 3.5 ps process does not result in loss of excited states. We therefore assign this 3.5 ps redshift to a diffusive solvation process of the excited 7-hydroxy-coumarin-3-carboxylic acid chromophore in the PYP protein matrix. We note that in PYP at neutral pH, a slight but progressive redshifting of the EAS takes place on picosecond timescales, but we cannot exclude that this is related to heterogeneity that exists in the ground state. The 51 ps component in locked PYP accounts for almost all of the fluorescence decay (dashed line in Fig. 3), although measurements at time bases of 800 ps and 2.2 ns (not shown) corroborate that a small fraction of the fluorescence decay also occurred at longer lifetimes of 0.33 and 3.77 ns. These lifetimes are in agreement with the 58 ps (75%), 0.45 ns (9%) and 3.4 ns (16%) reported in (28).

## Bacteriorhodopsin mutant D85S

Bacteriorhodopsin (bR) is a well-known light-driven proton pump found in the purple membrane of the archaeon *Halobacterium salinarum*. Upon illumination, bR translocates protons toward the exterior of the cell (for a recent review, see [32]). It binds retinal as a chromophore, which assumes an all-*trans* geometry in the ground state, and exhibits a *trans*-cis isomerization upon optical excitation. This event triggers a series of intraprotein proton transfers, accompanied by distinct and discrete structural changes in the protein, and ultimately a proton is pumped across the membrane. The resulting transmembrane proton gradient in turn drives ATP synthesis through the action of ATP synthase. BR undergoes a light-induced photocycle involving discrete reaction intermediates referred to as K, L, etc. through O, after which the protein returns to its all-*trans*-retinal ground state. The K intermediate corresponds to the 13-cis isomerized form of retinal, and is formed at 65% efficiency (32). The excited-state lifetime of bR is extremely short, with the major part of the excited-state decay occurring in the 200-500 fs time range and a minor fraction decaying in 1–2 ps (7,33–35). Recent ultrafast infrared experiments have shown that concomitant with the excited-state decay, isomerization of the retinal chromophore takes place (35).

The replacement of the aspartate by a serine in the D85S mutant leads to significant alterations of the functional and spectroscopic properties of the protein. In wild-type bR, the carboxyl group of Asp85 is negatively charged at physiological pH (32). In the D85S mutant, the serine at this position is neutral, which results in a redshifted absorption spectrum and a deep-blue color. The spatial structure of the blue D85S mutant was determined to a resolution of 2.25 Å (15), and indicated that the retinal chromophore adopts an all-*trans*-geometry. However, it could not be excluded that a small fraction of the chromophores exist in a 13-cis configuration.
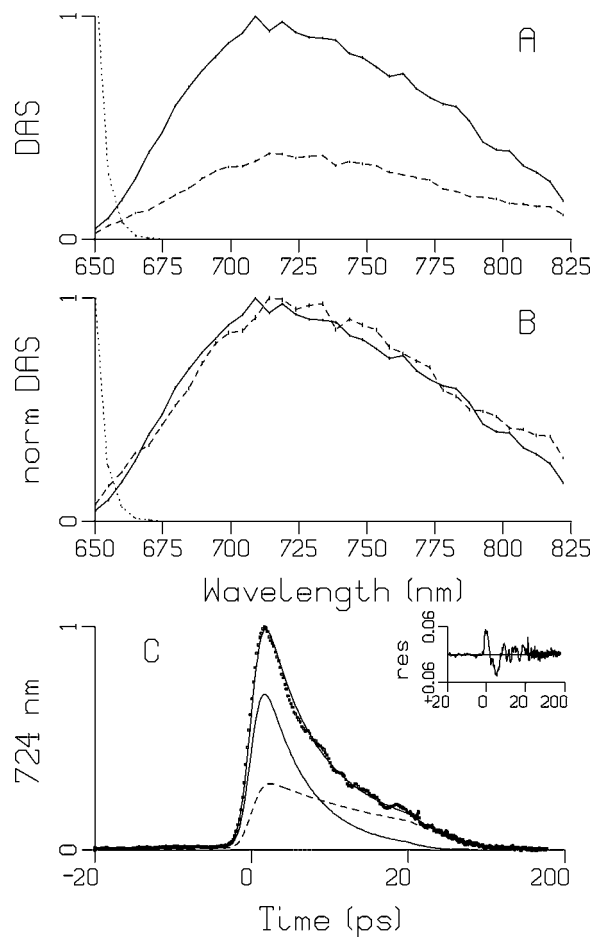


**Figure 4.** Results from global analysis of bacteriorhodopsin mutant D85S excited at 635 nm. (A) Decay-associated spectra (DAS). (B) Normalized DAS. Key: 5.2 ps (solid), 19.1 ps (dashed), scatter (dotted). (C) Fit of (normalized) kinetics measured at 724 nm. Inset shows residuals of a fit with two lifetimes. The contributions of these components to the fit are depicted by different line types. The time base is linear from −20 to +20 ps (relative to the maximum of the IRF), and logarithmic from 20 to 200 ps.

As shown before, the D85S mutant has a significantly longer excited-state lifetime with respect to wild-type bR, similar to acid blue or deionized bR, which has lifetimes in the order of 3.5 and 15 ps (7). This renders the D85S mutant very suitable to study diffusive solvation processes in the protein matrix in response to excitation of the retinal chromophore.

The bacteriorhodopsin mutant D85S was excited at 635 nm, which is on the low-energy side relative to the absorption maximum at 609 nm. The estimated DAS are depicted in Fig. 4A,B. At 650 nm some scatter is present (dotted). The emission clearly decays biexponentially (Fig. 4C), with estimated lifetimes of 5.2 and 19.1 ps, the latter representing a minor contribution. These values are consistent with previous pump-probe results (7) where lifetimes of 3.5 ps (65%) and 15 ps (35%) were found. Possible origins of the biexponentiality are heterogeneity of the pigment–protein complex, or (partial) relaxation to a longer-lived excited state. We note that in light-adapted wild-type bR, a pronounced bi- or multiexponential decay of the excited state has been detected as well (7,33,34). The 19.1 ps DAS (dashed in Fig. 4B) is slightly redshifted by about 120 cm$^{-1}$ relative to the 5.2 ps DAS (solid). The estimated $\bar{\nu}_{av}$ were both $13.0 \times 10^3$ cm$^{-1}$, and the FWHM was
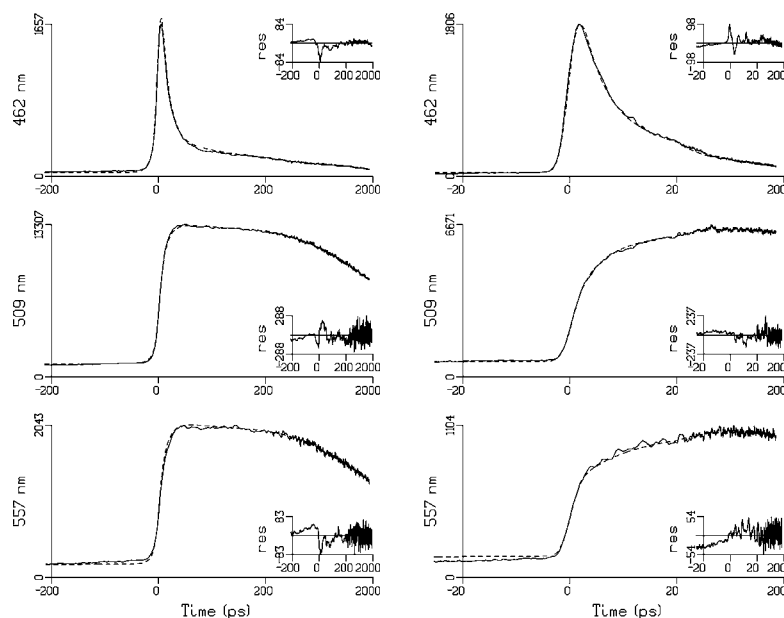
**Figure 5.** Results from global analysis of wtGFP excited at 400 nm. Fit of kinetics measured at 462, 509, and 557 nm (indicated at the ordinate). Excitation and detection were parallel. The dashed line represents a fit based upon five lifetimes: 3.2 ps, 11.6 ps, 111 ps, 1.33 ns and 2.59 ns. Insets show residuals of this fit. The time base (relative to the maximum of the IRF) is linear from −200 to +200 ps (left hand side) or −20 to +20 ps (right-hand side) and logarithmic at longer times.

$2540 \ cm^{-1}$, which is somewhat smaller than the width estimated from the steady-state spectrum (7). According to the heterogeneity explanation this would be attributable to longer-lived state(s) with a slightly lower transition energy.

The time-resolved streak camera data reveal that during the excited-state lifetime, no significant spectral shift of the emission maximum takes place in the D85S mutant of bacteriorhodopsin. This result is consistent with transient-absorption experiments on this protein, which showed no rise components of the stimulated emission at the red edge of the emission band (7). This indicates that the Stokes shift of the D85S mutant occurs within our time resolution of ~0.2 ps, and no or very little diffusive solvation processes occur on picosecond timescales. We may conclude that the Stokes shift exclusively arises from a very fast inertial response and the coupling to intramolecular vibrations of retinal.

**Green fluorescent protein**

During the last decade, GFP has become the fluorescent label of choice in cell biology and in many other research fields (36). GFP absorbs primarily in the near-UV but fluoresces in the green, and it is widely believed that the large shift of the emission to longer wavelengths after near-UV absorption is caused by a deprotonation reaction in the excited state of the neutral chromophore (37). The absorption spectrum of GFP exhibits a main absorption band near 400 nm, belonging to state A, and a minor band at 480 nm, belonging to state B (36). A corresponds to a state of the protein wherein the chromophore assumes a neutral form and B to a state with a deprotonated anionic chromophore. Upon excitation of the A band with near-UV light, the chromophore deprotonates on a picosecond time scale, and subsequent proton transport occurs, most likely via a hydrogen-bonded network that involves an internal water molecule, a serine residue, and as a terminal proton acceptor, an ionized glutamate (37–39). The thus-formed intermediate state, with a deprotonated anionic chromophore and a protonated neutral glutamate, is generally referred to as I* and is the emitting state of GFP. After radiative decay of I*, the proton is shuttled back to the chromophore in 400 ps (40). Despite GFP's obvious significance for biological investigations, our knowledge of the precise dynamic events that occur in the excited state have remained rather sketchy. With fluorescence-upconversion spectroscopy, it was shown that excited-state proton transfer took place with time constants of 3 and 12 ps (37). Time-correlated photon-counting experiments confirmed this assignment (41). In essence,
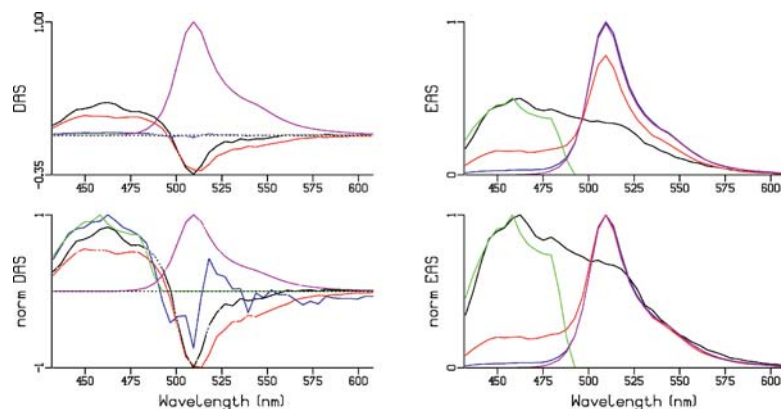


**Figure 6.** Evolution-associated spectra (EAS) estimated by applying a branched sequential scheme to wtGFP data for excitation at 400 nm: 1→2→3→4 (1.7%) and 1→2→3→5 (98.3%), with five lifetimes: 3.2 ps (black), 11.6 ps (red), 111 ps (blue), 1.33 ns (green), and 2.59 ns (magenta). (see Figure 5 for representative traces of the data). The DAS have been calculated from the EAS. Further explanation in text.
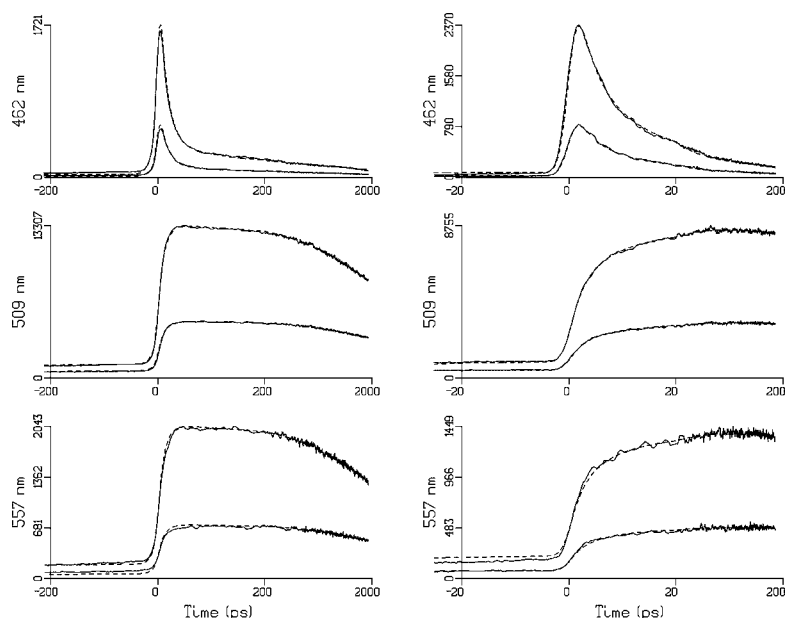
**Figure 7.** Results from target analysis of wt GFP excited at 400 nm. Fit of kinetics measured at 462, 509, and 557 nm (indicated at the ordinate). Excitation was parallel (upper curve) or perpendicular (lower curve). Dashed line represents fit based upon target model (explained in text) resulting in lifetimes of 2.7, 9.9, and 73 ps, 1.5 and 2.8 ns. The time base (relative to the maximum of the IRF) is linear from −200 to +200 ps (left-hand side) or −20 to +20 ps (right-hand side) and logarithmic at longer times.

the lack of spectrally resolved kinetic information precluded a detailed view of the excited-state processes in GFP in these studies. A detailed femtosecond transient-absorption study with broadband white-light detection revealed, for the first time, important aspects of the spectral evolution of GFP's excited states (42). However, it was shown later that evolution on the ground-state potential energy surface made a small but significant contribution to the dynamics (40). Here, we present a time- and spectrally resolved study of the excited-state dynamics in GFP with an IRF of 3.5 ps.

GFP emission upon 400 nm excitation was measured on a short (200 ps) and on a long time base (2.2 ns). The IRF widths were approximately 3.5 and 14 ps FWHM for the respective time bases. Typical traces and fits (with parallel detection) are shown in Fig. 5. The decay of A* at 462 nm, and accompanying rise of I* at 509 and 562 nm are clearly visible. Notice that long-lived emissions, as represented by the prezero signals caused by the backsweep (6), are present at all wavelengths. This indicates that next to the ~3 ns lifetime of I* also a minor fraction of A* decays with a ns lifetime. The decay of A* at 462 nm is multiexponential, as is the rise of I*. We found no indication for B* emission, and also no clear evidence for solvation of A*. To describe these data, five lifetimes were needed. Evolution-associated spectra (EAS) have been estimated with the use of a branched sequential scheme: 1→2→3→5 (98%) and 1→2→3→4 (1.7%, the minor fraction of A* that decays with a ns lifetime), where 1–5 indicates the order of the lifetimes. The fourth and fifth lifetime represent, respectively, the longest lifetime of A*, and the lifetime of I*. The EAS are shown in Fig. 6. The black EAS decays in 3.2 ps, forming the red EAS, which in 11.6 ps evolves into the blue EAS. The blue EAS lives for 111 ps, thereby forming the green EAS (1.33 ns, 1.7%) and the magenta EAS (2.59 ns, 98.3%). To resolve the two long lifetimes and EAS, the fourth EAS (green, representing long-lived A*) is assumed to be zero above 490 nm, whereas the fifth EAS (magenta, representing I*) is assumed to be zero below 460 nm. The first, second, and third EAS contain mixtures of A* and I*, with decreasing contribution of A* in time. The red tail of the first EAS (black) indicates that the time zero spectrum contains an I* contribution. This can be due to the presence of a small fraction of I

in the ground state, or to so-called cross-well excitation (37,42). The second EAS (red) indicates that ~60% of A* has already formed I* in 3.2 ps, whereas most of the remainder forms I* in 11.6 ps. This I* formation is also clear from the negative DAS amplitudes (black and red) above 500 nm. Less than 10% of A*
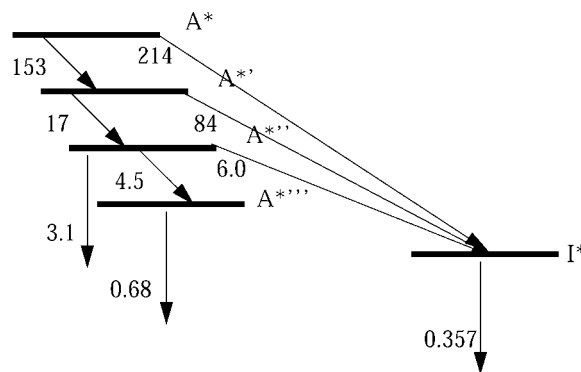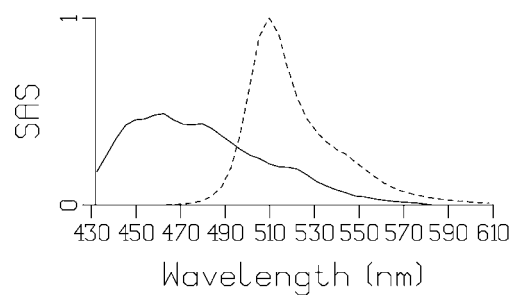




**Figure 8.** Species-associated spectra (SAS) of A* (solid) and I* (dashed) resulting from target analysis of wtGFP excited at 400 nm (see Fig. 7 for representative traces of the data). Kinetic scheme shows A* relaxation, with gradually decreasing probability of forming I*. Six percent of I* was formed instantaneously. Rate constants are in ns$^{-1}$. Lifetimes of A* are 2.7, 9.9, and 73 ps, 1.5 ns. Lifetime of I* 2.8 ns. Further explanation in text.

**Table 1.** Summary of results.

| Sample | $\lambda_{max}$abs,em (nm) | $\lambda_{exc}$ (nm) | Lifetimes (ps) | Interpretation |
|---|---|---|---|---|
| wtPYP, pH 7.5 | 446,494 (25) | 400 | ~0.25 | IVR, inertial solvation |
| | | | 1.7, 7.7 | Photochemistry, decay to GSI |
| | | | 30, 125 | Decay to GSI |
| wtPYP, pH 2 | 360,439 (22) | 377 | 2.1 | Solvation, decay to GSI |
| | | | 10, 34, 149 | Decay to GSI |
| Locked PYP, pH 7.5 | 443,465 (28) | 400 | ~0.1 | IVR, inertial solvation |
| | | | 3.5 | Diffusional solvation |
| | | | 51, 330, 3770 | Decay to GSI |
| bR D85S, pH 6 | 609,760 (7) | 635 | 5.2, 19.1 | Photochemistry, decay to GSI |
| GFP, pH 8 | A: 400,460 (Fig. 8) | 400 | 2.7, 9.9 | Photochemistry |
| | | | 73 | Photochemistry, decay to A |
| | | | 1500 | Decay to A |
| | I: 500,509 (40) | | 2800 | Decay to I |

decays in 111 ps, whereby it is not clear whether I* is formed; compare the noisy rise in the shape of the normalized blue DAS. On the assumption that the blue edge of the green EAS possesses a similar amplitude as the black EAS, it was found that about 1.7% of A* decays with 1.33 ns. In the region where A* and I* emission overlap, it becomes virtually impossible to estimate the green EAS. It is a recurring theme that the multiexponential decay of A* can have different explanations, that is, ground-state heterogeneity of A, or relaxation of A* with a gradually decreasing probability of forming I*. The latter explanation was advocated by Vöhringer *et al.* (42). We extended their model to accommodate the four observed A* decay times and performed a target analysis of our fluorescence anisotropic data (Fig. 7). The kinetic scheme is depicted in Fig. 8. The multiexponential decay of A* contains four lifetimes, with gradually decreasing probability of forming I*, and with two different rates of decay to the ground state. This was already clear from the blue and green DAS in Fig. 6, and points to heterogeneity. A small part of I* (6%) is formed instantaneously, and I* decays with the fifth lifetime.

To model the fluorescence anisotropy as well, this model was then extended with an anisotropy for A* or I* of the form $r(0)\exp(-t/\phi)$, with initial anisotropy $r(0)$ and rotational correlation time $\phi$ fixed at 15 ns (43). We assume that the A* SAS does not evolve, and is zero above 580 nm. Note that in this target analysis the five EAS from the global analysis are replaced by two SAS for A* and I*, an initial I* fraction, and four additional branching ratios, which is a large reduction in the number of free parameters. The estimated initial anisotropies are 0.39 and 0.38 for A* or I*, respectively. Comparing the estimated A* SAS (Fig. 8A, solid) with the time-zero spectrum (black EAS in Fig. 6), we note that after subtraction of the small (6%) initial I* contribution a well-shaped SAS results, which resembles a shifted P4-3 mutant spectrum, which is not photoactive (36). The estimated I* SAS resembles the long-lived DAS and EAS of Fig. 6, which were already satisfactory. We conclude that this target analysis satisfactorily describes 160.000 data points (partly shown in Fig. 7) with realistic SAS, with the use of a kinetic scheme that points to heterogeneity and maybe also to relaxation of A*.

## CONCLUSION

In all three systems studied multiexponential decay of emission was present, suggesting that ground-state heterogeneity is a common feature of these chromophore-protein complexes. Table 1 collates the results. In PYP parallel but different forms of photochemistry were demonstrated in (29,30), and also the internal conversion to a ground-state intermediate is most probably heterogeneous, as evidenced from the locked PYP emission. After excitation on the high-energy side, a large redshift of the emission was demonstrated in PYP on timescales of about 0.1 ps (solid EAS in Fig.1C [wtPYP] and in Fig. 3D [locked PYP]), which could be attributed to intramolecular vibrational relaxation (IVR) as well as to inertial solvation due to small amplitude motions of charges and dipoles (7). In addition, in locked PYP diffusive solvation was present on a timescale of 3.5 ps. In D85S and in wtPYP in the pBdark state the excitation was on the low-energy side, and no subpicosecond redshift of the emission was observed. Neither did we observe a redshift of the A* emission in GFP. The lack of observed solvation phenomena on a subpicosecond and picosecond timescale in GFP or D85S might be explained by the fact that the chromophore is buried more deeply in the protein than with PYP. With the use of target analysis, in GFP we demonstrated heterogeneity of photochemistry, with a gradually decreasing probability of forming I*.

## REFERENCES

1. Jimenez, R., G. R. Fleming, P. V. Kumar and M. Maroncelli (1994) Femtosecond solvation dynamics of water. *Nature* **369**, 471–473.
2. Horng, M. L., J. A. Gardecki, A. Papazyan and M. Maroncelli (1995) Subpicosecond measurements of polar solvation dynamics: coumarin 153 revisited. *J. Phys. Chem.* **99**, 17311–17337.
3. Fleming, G. R. and M. Cho (1996) Chromophore-solvent dynamics. *Annu. Rev. Phys. Chem.* **47**, 109–134.
4. Pal, S. K., J. Peon and A. H. Zewail (2002) Biological water at the protein surface: Dynamical solvation probed directly with femtosecond resolution. *Proc. Natl. Acad. Sci. USA* **99**, 1763–1768.
5. Haran, G., K. Wynne, A. Xie, Q. He, M. Chance and R. M. Hochstrasser (1996) Excited state dynamics of bacteriorhodopsin revealed by transient stimulated emission spectra. *Chem. Phys. Lett.* **261**, 389–395.
6. Petushkov, V. N., I. H. M. van Stokkum, B. Gobets, F. van Mourik, J. Lee, R. van Grondelle and A. J. W. G. Visser (2003) Ultrafast fluorescence relaxation spectroscopy of 6,7-dimethyl-(8-ribityl)-lumazine and riboflavin, free and bound to antenna proteins from bioluminescent bacteria. *J. Phys. Chem. B* **107**, 10934–10939.

7. Kennis, J. T. M., D. S. Larsen, K. Ohta, M. T. Facciotti, R. M. Glaeser and G. R. Fleming (2002) Ultrafast protein dynamics of bacteriorhodopsin probed by photon echo and transient absorption spectroscopy. *J. Phys. Chem. B* **106**, 6067–6080.

8. Homoelle B. J., M. D. Edington, W. M. Diffey and W. F. Beck (1998) Stimulated photon- echo and transient-grating studies of protein-matrix solvation dynamics and interexciton-state radiationless decay in alpha phycocyanin and allophycocyanin. *J. Phys. Chem. B* **102**, 3044–3052.

9. Jordanides, X. J., M. J. Lang, X. Y. Song and G. R. Fleming (1999) Solvation dynamics in protein environments studied by photon echo spectroscopy. *J. Phys. Chem. B* **103**, 7995–8005.

10. Changenet-Barret, P., C. Choma, E. Gooding, W. DeGrado and R. M. Hochstrasser (2000) Ultrafast dielectric response of proteins from dynamics Stokes shifting of coumarin in calmodulin. *J. Phys. Chem. B* **104**, 9322–9329.

11. Pierce, D. W. and S. G. Boxer (1992) Dielectric-relaxation in a protein matrix. *J. Phys. Chem.* **96**, 5560–5566.

12. Gobets, B., I. H. M. van Stokkum, M. Rögner, J. Kruip, E. Schlodder, N. V. Karapetyan, J. P. Dekker and R. van Grondelle (2001) Time-resolved fluorescence emission measurements of photosystem I particles of various cyanobacteria. A unified compartmental model. *Biophys. J.* **81**, 407–424.

13. Meyer, T. E. (1985) Isolation and characterization of soluble cytochromes, ferredoxins and other chromophoric proteins from the halophilic phototrophic bacterium *Ectothiorhodospira halophila*. *Biochim. Biophys. Acta* **806**, 175–183.

14. Hoff, W. D., I. H. M. van Stokkum, H. J. van Ramesdonk, M. E. van Brederode, A. M. Brouwer, J. C. Fitch, T. E. Meyer, R. van Grondelle and K. J. Hellingwerf (1994) Measurement and global analysis of the absorbance changes in the photocycle of the photoactive yellow protein from *Ectothiorhodospira halophila*. *Biophys. J.* **67**, 1691–1705.

15. Rouhani, S., J. P. Cartailler, M. T. Facciotti, P. Walian, R. Needleman, J. K. Lanyi, R. M. Glaeser and H. Luecke (2001) Crystal structure of the D85S mutant of bacteriorhodopsin: model of an O-like photocycle intermediate. *J. Mol. Biol.* **313**, 615–628.

16. Nagle, J. F., L. A. Parodi and R. H. Lozier (1982) Procedure for testing kinetic-models of the photocycle of bacteriorhodopsin. *Biophys. J.* **38**, 161–174.

17. Van Stokkum, I. H. M., D. S. Larsen and R. van Grondelle (2004) Global and target analysis of time resolved spectra. *Biochim. Biophys. Acta* **1657**, 82–104, and **1658**, 262 (Erratum).

18. Vilchiz, V. H., J. A. Kloepfer, A. C. Germaine, V. A. Lenchenkov and S. E. Bradforth (2001) Map for the relaxation dynamics of hot photoelectrons injected into liquid water via anion threshold. Photodetachment and above threshold solvent ionization. *J. Phys. Chem. A* **105**, 1711–1723.

19. Vengris, M., M. A. van der Horst, G. Zgrablić, I. H. M. van Stokkum, S. Haacke, M. Chergui, K. J. Hellingwerf, R. van Grondelle and D. S. Larsen (2004) Contrasting the excited-state dynamics of the photoactive yellow protein chromophore: protein vs. solvent effects. *Biophys. J.* **87**, 1848–1857.

20. Hellingwerf, K. J., J. Hendriks and T. Gensch (2003) Photoactive yellow protein, a new type of photoreceptor protein: Will this "yellow lab" bring us where we want to go? *J. Phys. Chem. A* **107**, 1082–1094.

21. Cusanovich, M. A. and T. E. Meyer (2003) Photoactive yellow protein, a prototypic PAS domain sensory protein and development of a common signaling mechanism. *Biochemistry* **42**, 4759–4770.

22. Kroon, A. R., W. D. Hoff, H. P. M. Fennema, J. Gijzen, G. J. Koomen, J. W. Verhoeven, W. Crielaard and K. J. Hellingwerf (1996) Spectral tuning, fluorescence, and photoactivity in hybrids of photoactive yellow protein, reconstituted with native or modified chromophores. *J. Biol. Chem.* **271**, 31949–31956.

23. Van Brederode, M. E., W. D. Hoff, I. H. M. van Stokkum, M. L. Groot and K. J. Hellingwerf (1996) Protein folding thermodynamics applied to the photocycle of photoactive yellow protein. *Biophys. J.* **71**, 365–380.

24. Van der Horst, M. A. and K. J. Hellingwerf (2004) Photoreceptor proteins, "star actors of modern times": A review of the functional dynamics in the structure of representative members of six different photoreceptor families. *Acc. Chem. Res.* **37**, 13–20.

25. Meyer, T. E., G. Tollin, T. P. Causgrove and R. E. Blankenship (1991) Picosecond decay kinetics and quantum yield of fluorescence of the photoactive yellow protein from the halophilic purple phototrophic bacterium *Ectothiorhodospira halophila*. *Biophys. J.* **59**, 988–991.

26. Baltuška, A., I. H. M. van Stokkum, A. Kroon, R. Monshouwer, K. J. Hellingwerf and R. van Grondelle, (1997) The primary events in the photoactivation of yellow protein. *Chem. Phys. Lett.* **270**, 263–266.

27. Chosrowjan, H., N. Mataga, N. Nakashima, Y. Imamoto and F. Tokunaga (1997) Femtosecond-picosecond fluorescence studies on excited state dynamics of photoactive yellow protein from *Ectothiorhodospira halophila*. *Chem. Phys. Lett.* **270**, 267–272.

28. Changenet, P., H. Zhang, M. J. van der Meer, K. J. Hellingwerf and M. Glasbeek (1998) Subpicosecond fluorescence upconversion measurements of primary events in yellow proteins. *Chem. Phys. Lett.* **282**, 276–282.

29. Groot, M. L., L. J. G. W. van Wilderen, D. S. Larsen, M. A. van der Horst, I. H. M. van Stokkum, K. J. Hellingwerf and R. van Grondelle (2003) Initial steps of signal generation in photoactive yellow protein revealed with femtosecond mid-infrared spectroscopy. *Biochemistry* **42**, 10054–10059.

30. Larsen, D. S., I. H. M. van Stokkum, M. Vengris, M. A. van der Horst, F. L. de Weerd, K. J. Hellingwerf and R. van Grondelle (2004) Incoherent manipulation of the photoactive yellow protein photocyle with dispersed pump-dump-probe spectroscopy. *Biophys. J.* **87**, 1858–1872.

31. Ujj, L., S. Devanathan, T. E. Meyer, M. A. Cusanovich, G. Tollin and G. H. Atkinson (1998) New photocycle intermediates in the photoactive yellow protein from *Ectothiorhodospira halophila*: picosecond transient absorption spectroscopy. *Biophys. J.* **75**, 406–412.

32. Lanyi, J. K. (2000) Molecular mechanism of ion transport in bacteriorhodopsin: insights from crystallographic, spectroscopic, kinetic, and mutational studies. *J. Phys. Chem. B* **104**, 11441–11448.

33. Du, M. and G. R. Fleming (1993) Femtosecond time-resolved fluorescence spectroscopy of bacteriorhodopsin—direct observation of excited-state dynamics in the primary step of the proton pump cycle. *Biophys. Chem.* **48**, 101–111.

34. Hasson, K. C., F. Gai and P. A. Anfinrud (1996) The photoisomerization of retinal in bacteriorhodopsin: experimental evidence for a three-state model. *Proc. Natl. Acad. Sci. USA* **93**, 15124–15129.

35. Herbst, J., K. Heyne and R. Diller (2002) Femtosecond infrared spectroscopy of bacteriorhodopsin chromophore isomerization. *Science* **297**, 822–825.

36. Tsien, R. Y. (1998) The green fluorescent protein. *Annu. Rev. Biochem.* **67**, 509–544.

37. Chattoraj, M., B. A. King, G. U. Bublitz and S. G. Boxer (1996) Ultrafast excited state dynamics in green fluorescent protein: Multiple states and proton transfer. *Proc. Natl. Acad. Sci. USA* **93**, 8362–8367.

38. Stoner-Ma, D., A. A. Jaye, P. Matousek, M. Towrie, S. R. Meech and P. J. Tonge (2005) Observation of excited-state proton transfer in green fluorescent protein using ultrafast vibrational spectroscopy. *J. Am. Chem. Soc.* **127**, 2864–2865.

39. Yang, F., L. G. Moss and G. N. Phillips (1996) The molecular structure of green fluorescent protein. *Nat. Biotechnol.* **14**, 1246–1251.

40. Kennis, J. T. M., D. S. Larsen, I. H. M. van Stokkum, M. Vengris, J. J. van Thor and R. van Grondelle (2004) Uncovering the hidden ground state of green fluorescent protein. *Proc. Natl. Acad. Sci. USA* **52**, 17988–17993.

41. Lossau, H., A. Kummer, R. Heinecke, F. Pollinger-Dammer, C. Kompa, G. Bieser, T. Jonsson, C. M. Silva, M. M. Yang, D. C. Youvan and M. E. Michel-Beyerle (1996) Time- resolved spectroscopy of wild-type and mutant green fluorescent proteins reveals excited state deprotonation consistent with fluorophore-protein interactions. *Chem. Phys.* **213**, 1–6.

42. Winkler, K., J. R. Lindner, V. Subramaniam, T. M. Jovin and P. Vöhringer (2002) Ultrafast dynamics in the excited state of green fluorescent protein (wt) studied by frequency- resolved femtosecond pump-probe spectroscopy. *Phys. Chem. Chem. Phys.* **4**, 1072–1081.

43. Striker, G., V. Subramaniam, C. A. M. Seidel and A. Volkmer (1999) Photochromicity and fluorescence lifetimes of green fluorescent protein. *J. Phys. Chem. B* **103**, 8612–8617.